DOI: 10.1002/chem.200600403

Molecular Recognition: Preorganization of a Bis(pyrrole) Schiff Base Derivative for Tight Dimerization by Hydrogen Bonding

Orde Q. Munro,* Sandra D. Joubert, and Craig D. Grimmer[a]

Abstract: Multiple techniques have been used to delineate the self-assembly of a bis(pyrrole) Schiff base derivative (compound **4**, $C_{16}H_{14}N_4$), which forms an unusual dimer through complementary N−H···N=C hydrogen bonds between twisted, C_2-symmetric monomer units. The asymmetric unit of the crystal structure comprises one and a half dimer units, with one dimer exhibiting approximate D_2 point-group symmetry and the other exact D_2 symmetry (space group $C2/c$). The dimers pack into columns whose axes are collinear with the a axis of the unit cell. The columns assemble into discrete layers with two distinct types of hydrogen-sized voids residing between the layers. Despite the promising architecture of the voids within the lattice of **4**, the absence of genuine channels to interconnect the voids precludes the uptake of hydrogen gas, even at elevated pressures (10 bar). AM1 calculations of the structure of dimeric **4** indicate that self-recognition through hydrogen bonding depends primarily on favorable electrostatic interactions. The potential-energy surface for monomeric **4** mapped by counter-rotation of an adjacent pair of C=C-N=C torsion angles indicates that the X-ray structures of the four monomeric units are global minima with highly nonplanar conformations that are preorganized for self-recognition by hydrogen bonding. The in vacuo enthalpy of association for the dimer was calculated to be significantly exergonic ($\Delta G_{assoc} = -21.9$ kJ mol^{-1}, 298 K) and in excellent agreement with that determined by ^{1}H NMR spectroscopy in $CDCl_3$ ($\Delta G_{assoc} = -16.6(4)$ kJ mol^{-1}, 298 K). Using population and bond order analyses, in conjunction with the conformation dependence of the frontier MO energies, we have been able to show that π-electron delocalization is only marginally diminished in the nonplanar conformers of **4** and that the electronic structures of the constituent monomers of the dimer are well mixed.

Keywords: dimerization · hydrogen bonds · molecular recognition · Schiff bases · self-assembly

Introduction

Bis(pyrrole) Schiff base derivatives **1** (Scheme 1), where X is a synthetically variable bridging alkyl or aryl group, have been known since the 1960s.[1] Despite their long existence, however, relatively few crystal structures of metal-free or metalated tetradentate ligands have been reported. Metal ions are usually coordinated by **1** as the dianionic conjugate base (structure type **2**, where M is a divalent or trivalent metal ion). Examples of crystallographically characterized complexes of type **2** include chelates of Ru^{II},[2] Pd^{II},[3] Ni^{II},[4] Cu^{II},[5] Mn^{II},[6,7] Fe^{II},[7] Sm^{II},[8] and Co^{III}.[9] Several dinuclear species of the type $[M_2(L)_2]$ are also known for $M = Zn^{II}$,[10] Mn^{II},[6] and Cu^{II}[5] where L is a derivative of type **1**. Indeed, by varying the bridging group X it is possible to control the supramolecular coordination chemistry of such systems. For example, Wu et al. have shown, using a substituted analogue of **1** with Zn^{II}, that when the linker is 1,2-, 1,3-, or 1,4-diaminobenzene, dinuclear, trinuclear $[M_3(L)_3]$, or porous tetranuclear complexes $[M_4(L)_4]$, respectively, are synthetically feasible.[10]

To date, studies of the coordination chemistry of analogues of **2** have not been paralleled to the same extent by structural and spectroscopic studies of the metal-free species. However, two independent articles[11,12] published in 2003 showed, in more than passing detail, that the pyrrole-imine functional group combination in **3** (Scheme 1 is a potentially useful supramolecular synthon comprising a strong H-bond donor (pyrrole N−H group) and a strong H-bond acceptor (imine nitrogen). Efficient self-recognition or self-assembly through complementary hydrogen bonding in this type of system is now known to lead to dimerization (**3a**)

[a] Prof. O. Q. Munro, S. D. Joubert, C. D. Grimmer
School of Chemistry, University of KwaZulu-Natal
Private Bag X01, Scottsville 3209, Pietermaritzburg (South Africa)
Fax: (+27) 33-260-5009
E-mail: munroo@ukzn.ac.za.

Supporting Information for this article is available on the WWW under http://www.chemeurj.org/ or from the author.

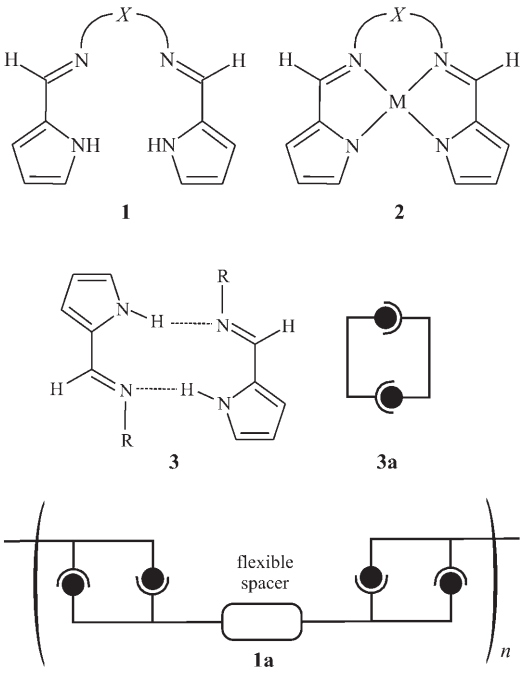

Scheme 1.

and polymerization (**1a**) in the case of mono- and bis-(pyrrole) derivatives, respectively.

For crystal engineering applications, small variations in the identity of the spacer, such as regioisomerism of the two amino groups on a diaminobenzene ring, allow one to elegantly control the supramolecular chemistry of the system, particularly if metal ions are used to facilitate oligomerization.[10] Although the simplest aromatic derivative of **1** with $X = C_6H_4$ (1,2-diaminobenzene-based spacer, compound **4**; Scheme 2) has been synthesized before, no crystal structure of the free base has been reported.[3,6] Surprisingly, only three derivatives of **1** have been crystallographically characterized, namely 4,5-dimethyl-*N*,*N*′-bis(1*H*-pyrrol-2-ylmethylene)benzene-1,2-diamine (**5**),[6] *N*,*N*′-bis(1*H*-pyrrol-2-ylmethylene)propane-1,2-diamine (**6**),[11] and *N*,*N*′-(1,2-cyclohexylene)bis(1*H*-pyrrol-2-ylmethyleneamine) (**7**).[3] Self-assembly occurs in **5** and **6** through hydrogen bonding, as depicted in **3/3a** (Scheme 1).[13]

The existing evidence suggests that a pyrrole group adjacent to an imine group constitutes a powerful molecular recognition motif with integral H-bond donor and acceptor sites. Furthermore, the addition of other H-bonding functional groups to such a system enhances the ability of these compounds to participate in molecular recognition events. For example, the mono(pyrrole) Schiff base derivative *N*-[(1*E*)-1*H*-pyrrol-2-ylmethylene)]benzene-1,2-diamine (**8**) self-assembles by complementary (pyrrole)N−H···NH_2Ar hydrogen bonding both in solution and in the solid state.[14] Crystal engineering applications of metal-free, pyrrole-imine Schiff bases are clearly at a very early stage of development, but have the potential to yield some useful new supramolecular architectures. Herein, we report the X-ray structural characterization of **4** (a tight H-bonded dimer), NMR studies which delineate the process of self-assembly in fluid solution, and gas-phase AM1 simulations of the electronic structures of the monomeric and dimeric species. Our data collectively show that complementary electrostatic interactions and conformational preorganization are two fundamental parameters that control highly favorable self-assembly in this system.

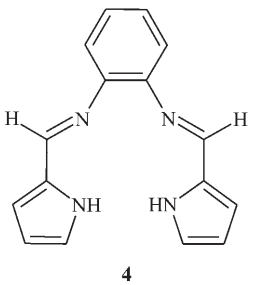

Scheme 2.

Results and Discussion

Solid-state molecular structures: The asymmetric unit of **4** comprises three molecules: two fully occupied molecules in general positions and two symmetry-unique half-molecules. (For convenience, the four independent structural components of the asymmetric unit are labeled A, B, C, and D.) Compound **4** therefore exists as discrete dimers in the crystalline solid state (Figure 1). The two half molecules labeled C and D are the symmetry-unique components of a dimer with D_2 point-group symmetry paired by complementary (pyrrole)N−H···N=C(imine) hydrogen bonding, while the fully occupied molecules A and B (C_1 symmetry) are similarly hydrogen-bonded to form a dimer with only approximate D_2 symmetry (the molecular point group is strictly C_1). For molecule B, the mean pyrrole α-C−N, α-C−β-C and β-C−β-C bond lengths are 1.369(7), 1.378(6), and 1.414(2) Å, respectively. The pair of imine C=N bond lengths average 1.278(1) Å, while the mean pyrrole α-C−(C=N) bond measures 1.441(4) Å. The mean C−C bond length of the phenyl ring is 1.396(8) Å. The mean bond angles subtended at the N atoms of **4** are 109.6(6)° (C-N-C), 124.8(13)° (H-N-C), and 118.3(6)° (C=N-CH_2). As might be anticipated from a reasonably good data set, these mean distances and angles compare favorably with those reported for similar derivatives of **1**.[3,6,11] The structural parameters for all four molecules (A–D) are similar, which obviates the need for further discussion of the key bond distances and angles for molecules A, C, and D.

Taking molecule B as being representative of each monomer in the asymmetric unit of **4**, it is clear that a markedly non-planar conformation is favored in this system; the dihedral angle between the mean plane of one pyrrole group and the adjacent pyrrole ring is 35.98(4)° (see Figure 2 and Figure S1 in the Supporting Information). The pyrrole rings themselves are twisted out of the molecular plane and the

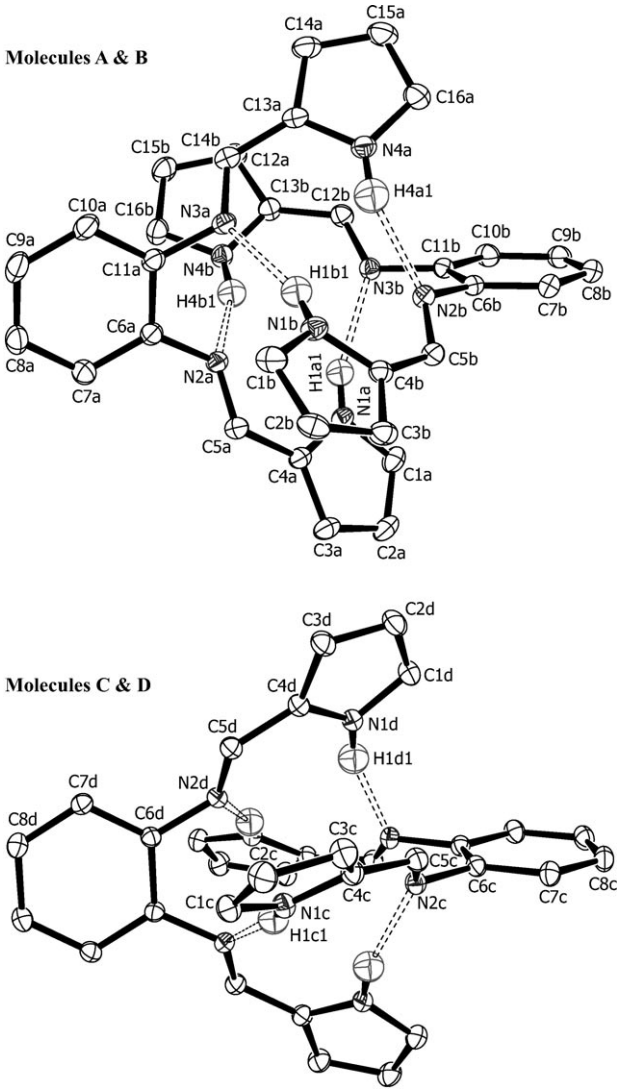

Figure 1. Thermal ellipsoid plots of the two independent dimer structures of **4** at 100(2) K. (Displacement ellipsoids are drawn at the 50% probability level; only the isotropically refined hydrogen atoms are shown for clarity.) Molecules A and B make up the first C_1-symmetric dimer; the component monomers are designated by lowercase letters a and b on all atom labels. The second dimer comprises independent half-molecules C and D and has exact D_2 symmetry. Hydrogen bonds are shown with broken lines in both H-bonded complexes.

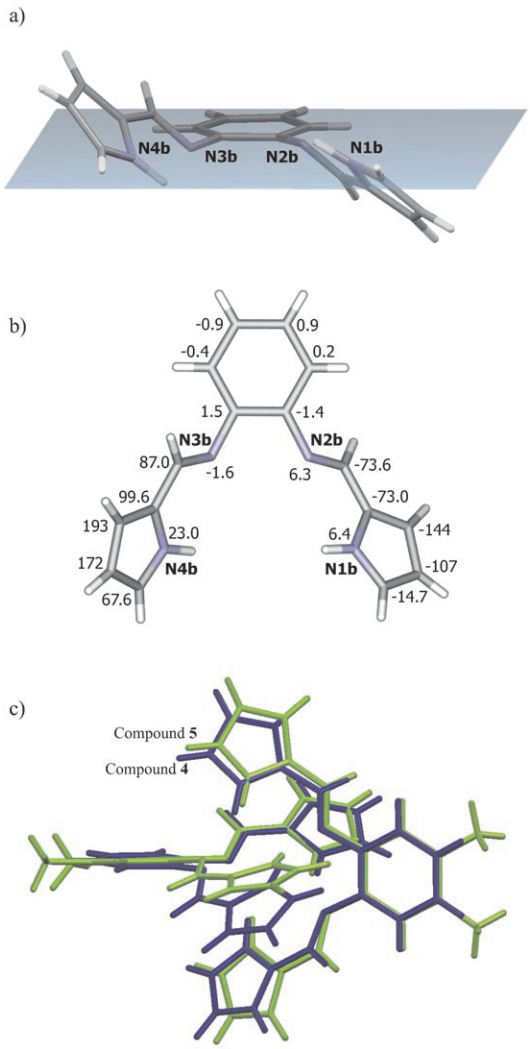

Figure 2. a) Representation of the mean plane passing through the benzene ring of **4** (molecule B); the sharply canted orientations of the pyrrole rings relative to this plane are clearly evident. b) Depiction of the perpendicular displacements of all non-hydrogen atoms of compound **4** from the six-atom mean plane of the benzene ring. Atomic displacements are given in units of 0.01 Å; standard uncertainties range from 0.001 to 0.004 Å. c) Least-squares fit of the benzene rings of the X-ray structures of **4** and **5** (RMSD = 1.81 Å). Compound **4** clearly has the more nonplanar conformation.

angle between the mean plane of the first pyrrole ring (containing atom N1b) and the mean plane through the phenyl ring is 42.70(6)°. This dihedral angle for the second pyrrole ring (including N4b) is a substantial −50.52(6)°. As shown in Figure 2, the perpendicular displacements of the non-hydrogen atoms of the structure from the six-atom mean plane of the central benzene ring range from 0 to 1.93(4) Å, thus highlighting the strikingly nonplanar conformation of the molecule.

The nonbonded distance between the N atoms of the pyrrole groups (N1b and N4b) is 5.273(1) Å. The complementary hydrogen bonds between the pyrrole NH groups of one molecule and the imine nitrogen atoms of the other (and vice versa) lock the two C-shaped structures almost perpendicularly together (the dihedral angle between the two 20-atom mean planes is 83(2)°, Figure 1). The average N–H-(pyrrole)···N(imine) hydrogen bond distance for **4** is 2.04(3) Å (Table 1), which is consistent with moderate to strong, rather than weak, hydrogen bonding.[15,16] The X-ray data therefore clearly indicate that the pyrrole N–H groups serve as hydrogen-bond donors and the imine groups as hydrogen-bond acceptors. Remarkably, complementary N–H···NR=CR_2 hydrogen bonding from an adjacent pair of pyrrole-imine functional groups and concomitant formation of ring motif **3** is, in fact, unusual, having hitherto escaped any rigorous statistical scrutiny.[17]

Table 1. Hydrogen bonding geometries for **4**.[a,b]

Interaction	D–H	H···A	D–H···A	D···A
N1a–H1a1···N3b	0.923(16)	2.050(16)	162(1)	2.943(2)
N1b–H1b1···N3a	0.940(18)	2.018(18)	159(2)	2.916(2)
N1c–H1c1···N2d[c]	0.904(17)	2.115(17)	164(2)	2.997(2)
N1d–H1d1···N2c[c]	0.920(17)	2.019(17)	159(2)	2.899(2)
N4a–H4a1···N2b	0.903(18)	2.035(18)	158(2)	2.892(2)
N4b–H4b1···N2a	0.940(17)	2.024(17)	155(1)	2.907(2)
average	0.92(1)	2.04(3)	160(3)	2.93(3)

[a] Distances in angstroms; angles in degrees. [b] D = donor; A = acceptor. [c] Symmetry code: $-x+1$, y, $-z+3/2$.

Just how tight is the complementary hydrogen bonding in **4**? A search of the CSD for derivatives of **3** revealed that, in the absence of unusual stereochemical constraints or included H-bonded solvent species, most of the available structures self-assemble in the solid state via the archetypal supramolecular synthon shown schematically in **3a**. The hydrogen-bonding parameters for seven compounds that show type **3** molecular recognition are summarized in Table 2.

Table 2. Summary of the mean hydrogen-bonding geometries for derivatives of **1** and **3** (structures are given in Figure S2).[a,b]

CSD ref. code	Structure[c]	Av. H···A	Av. D–H···A	Av. D···A
AWIXIN[12]	**7**, BP	2.26(33)	154(3)	2.910(4)
EMIHEN[11]	**6**, BP	2.066(6)	166(2)	2.942(6)
EWOLUX[d],[21]	**9**, MP	2.198	158	2.999
EWOMAE[d],[21]	**10**, MP	2.172	171	3.023
QOSMAM[6]	**5**, BP	2.10(3)	156(1)	2.93(3)
SUVMUR[d],[22]	**11**, MP	2.169(7)	166(1)	3.032(9)
UMUKUJ[d],[23]	**12**, MP	2.141	158	3.042
average	–	2.16(6)	161(5)	2.98(5)

[a] Distances in angstroms; angles in degrees. [b] D = donor; A = acceptor. [c] MP = mono(pyrrole), BP = bis(pyrrole). [d] One symmetry-unique hydrogen bond.

While it is generally recognized[16] that the strength of a hydrogen bond is not linearly dependent on the interaction distance,[18] we note that the mean hydrogen-bond distance for **4** is somewhat shorter than the average interaction distance given in Table 2.[19] This may well reflect the fact that **4** comprises two molecular recognition synthons **3** and forms a tightly interlocked dimer. Interestingly, Allen and coworkers[17] have analyzed the distribution of crystallographically determined distances for N–H···N interactions in the CSD and have reported that the most frequently observed hydrogen-bond distance for this type of interaction ranges from 2.033–2.066 Å; clearly, compound **4** falls neatly into this range with its 2.04(3) Å average. Furthermore, since most weak hydrogen bonds of the C–H···O type have interaction distances greater than 2.2 Å, we conclude that the X-ray structure of **4**, together with those listed in Table 2, exhibit structurally tight (i.e., intermediate to strong) hydrogen bonding.[20] The large association constant measured for **4** in solution by NMR spectroscopy (vide infra) independently supports this conclusion.

An intriguing feature of the X-ray structure of **4** is the non-coplanar arrangement of the pyrrole groups. At first glance, this conformation might be explained by the fact that **4** forms hydrogen-bonded dimers in the crystal lattice. Optimal binding of the monomers could dictate that each pyrrole ring twists out of the mean molecular plane, or so it may seem from the dimeric structure of **4** and the related 4,5-dimethylbenzene derivative **5**, which has a similar, though slightly less distorted, conformation (Figure 2c).[6] However, our AM1 simulation of the lowest-energy conformation of monomeric **4** in the gas phase clearly suggests that the very notion that this compound should be planar is *strictly incorrect* (vide infra). A nonbonded repulsion between the two pyrrole N–H groups in the planar conformer evidently drives the formation of the strain-relieving twisted structure for each monomer. Since this conformation differs insignificantly from that of molecule B in Figure 1, the X-ray structure of **4** essentially comprises four lowest-energy conformers of the compound. The twisted conformation of **4** (with exact or approximate D_2 point-group symmetry) therefore distinctly preorganizes the monomer for self-recognition by complementary intermolecular hydrogen bonding. Interestingly, according to MacGillivray's classification,[24] both **4** and **5** may be categorized as symmetric U-shaped bifunctional supramolecular synthons that are fundamentally capable of forming homodimers through H-bonding interactions.

Crystal packing: The crystal structure of **4** has a relatively large unit cell accommodating 24 molecules. Viewing the unit cell down the *a*-axis (Figure 3a) is somewhat deceptive as it suggests that molecular scale cavities (approximately 3.6 Å in diameter), created by association of the nonplanar monomers into dimeric structures and subsequent ordering of the dimers into columns along the *a* axis, might possibly exist. However, it is important to note that since a plot of the unit cell contents using van der Waals radii for the atoms almost completely fills these apparent cavities (Figure S3), the crystal structure is *not truly porous* (genuine infinite channels are absent). Studies on porous molecular crystals (particularly metal–organic frameworks) are currently highly topical.[25] Indeed, elegant work by Barbour and co-workers[26] suggests that *seemingly nonporous lattices* with no discernible channels (but discrete cavities or voids) may behave as porous materials that can reversibly absorb gases such as methane, halogens, CO_2, CO, and N_2.

Given the present global interest in finding molecular materials suitable for gas storage applications (particularly H_2),[27,28] we examined the crystal lattice of **4** a bit more closely. By using a probe radius of 1.2 Å (van der Waals radius of H) with MSROLL[29] interfaced to X-Seed,[30] we identified 16 voids belonging to two types (A and B) between the layers formed by the columns of dimers (Figure 3b and 3c). The first type of void (type A) has a volume of 15.3(1) Å^3 and has four sites per layer in the unit cell. The remaining 12 sites are type B voids that each comprise two closely spaced (2.22 Å separation) smaller voids of

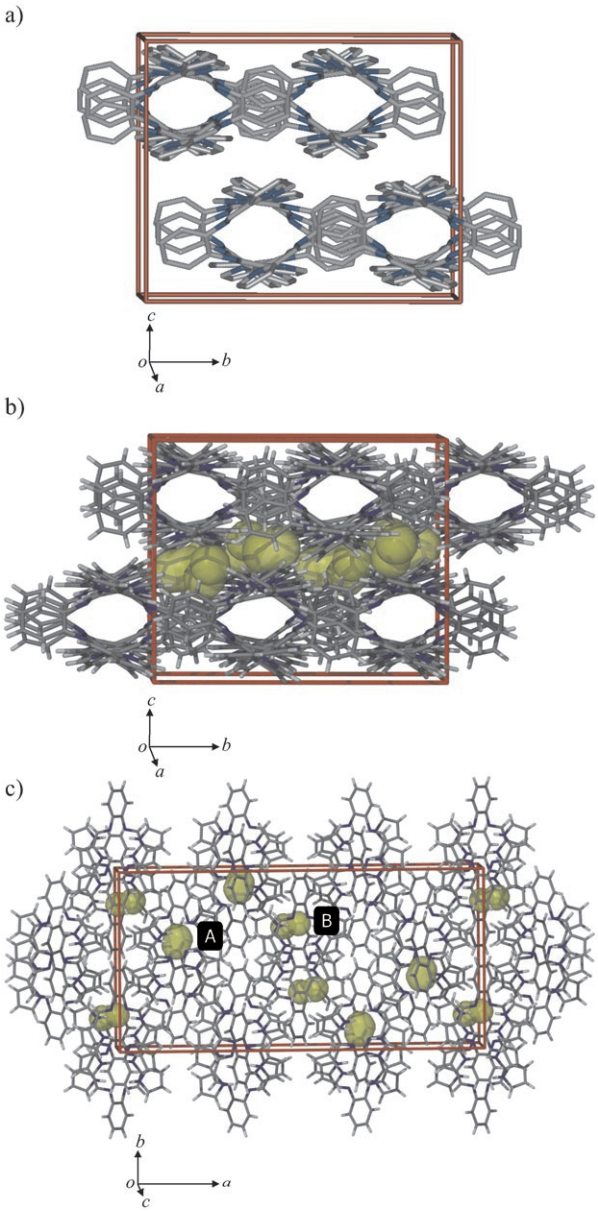

Figure 3. a) Unit cell contents for **4** viewed approximately down the *a* axis (hydrogen atoms have been omitted for clarity). b) Stick plot of the unit cell contents illustrating the locations of the voids (semi-transparent surfaces calculated with a grid point probe radius of 1.2 Å using MSROLL[29] interfaced to X-Seed[30]). c) Unit cell contents viewed approximately down the *c* axis illustrating the locations and shapes of the two types of voids.

7.6(0) and 8.3(0) Å^3. Since these smaller voids are overlapped, we have classified them as belonging to a single site B with a mean volume of around 15 Å^3. The distinction between the sites is clearly evident from the projection of the unit cell contents down the *c* axis (Figure 3c) as well as the *b* axis (Figure S4). Similar void sites were identified using OSCAIL-X's VOID algorithm,[31,32] but since the exact cavity volumes are not output by the program, it is somewhat less useful than MSROLL.

Encouraged by the existence of H_2-shaped cavities in the lattice of **4** (H_2 has a van der Waals volume of about 13 Å^3),[25] we tested the material for H_2 sorption. In a typical experiment, gas uptake was measured volumetrically[33] by monitoring the pressure drop as a function of time in a closed system containing the host material and the test gas at a known initial pressure. A pure sample of microcrystalline **4** (1.0 g) showed no H_2 uptake at an initial hydrogen pressure of about 1.3 bar. Experiments at higher initial hydrogen pressures (10 bar) also showed no hydrogen uptake. These data suggest that: a) the lack of genuine channels in the lattice inhibits hydrogen diffusion and thus its uptake in the "tailor-made" voids and/or b) a phase change that could possibly permit the uptake of H_2 cannot readily occur at ambient temperature, even at elevated hydrogen pressures.[34] In keeping with the idea that supramolecular aggregates can be tailored to produce functional materials,[24,35] it is foreseeable that U-shaped aromatic derivatives of **1** with more widely spaced H-bonding motifs **3** might well produce similar layers of H-bonded dimers within columnar stacks that encompass true infinite channels and harbor H_2-shaped voids in the interlayer sites. Such a material would presumably have the correct lattice architecture to permit both diffusion and storage of molecular hydrogen.

Despite the fact that solid **4** is not a true porous material, the packing shown in Figure 3a is nevertheless interesting, particularly since two layers of molecules exist, each of which consists of two adjacent rows or columns of stacked dimers. In the lower left row of molecules, the sequence of stacked dimers is C···D, A···B, A···B, and C···D. This column of molecules fits alongside a column of A···B, C···D, and A···B dimers in the same plane. The right-hand-side column of dimers is translated along the *a* axis to half the distance between any pair of dimers in the left column, thereby achieving relatively tight "bump-in-hollow" packing within the same layer. As might be anticipated from the space group symmetry, the upper layer is the inverse of the lower layer (the twofold axis runs co-linear with the *a* axis in the center of the unit cell, exactly midway between the two layers). In the interests of brevity, discussion of the most prominent short contacts involving dimer A···B and dimer C···D is given in the Supporting Information (Figure S5).

Solution ^{1}H NMR studies: To be regarded as a well-defined molecular recognition process, the formation of a hydrogen-bonded dimer in the solid state should be mirrored by the same event in fluid solution. One of the most accurate experimental methods available to delineate hydrogen-bonded molecular associations in solution is to probe the resonance frequencies of protons directly involved in the self-recognition process by high-field ^{1}H NMR spectroscopy.[36] Indeed, Steiner[20] has noted that X–H proton chemical shifts for an H-bond donor typically fall in the range $\delta = 14$–22 ppm in strongly H-bonded species and appear around $\delta = 14$ ppm in moderately H-bonded species. (These are only approximate values for the chemical shift ranges as the identities of the

H-bond donor, the solvent system, and the H-bond acceptor cannot be ignored.)

Chemical shifts versus concentration: We recorded the ^{1}H NMR spectrum of **4** as a function of concentration in $CDCl_3$ at 25 °C (Figure 4). The pyrrole N–H protons participate directly in the molecular recognition event as the hydrogen-bond donors in the dimeric structure of **4** (Figure 1) and this fact is clearly evident from the NMR spectra in the $\delta = 10$–13 ppm chemical shift range. More specifically, the pyrrole N–H proton signal increases in intensity (as expected) and shifts by 0.7 ppm downfield from $\delta = 11.8$ ppm to around $\delta = 12.5$ ppm with an increase in the concentration of **4** from 3.3 mM to 847 mM. The simplest model accounting for the self-assembly of **4** in fluid solution is one based on a dimerization process involving two monomers (M) combining to give the hydrogen-bonded dimer (D, Figure 5). If we assume that the observed chemical shift for the pyrrole N–H protons is the equilibrium-weighted average of the chemical shifts of the monomer and dimer, then a modified form of the usual dimerization equation[14] that takes into account nonspecific changes in the chemical shift with increasing solute concentration (i.e., perturbations *not* due to the dimerization process itself, such as monotonic changes in the dielectric constant of the medium) can be used to fit the concentration dependence of the signal (Equation (1)). In this equation the terms δ_{obs}, δ_M, and δ_D are the chemical shifts of the equilibrium mixture, monomer, and dimer, respectively, C_{tot} is the total concentration of **4**, and $\theta = d(\delta_{obs})/dC_{tot}$. The association (or dimerization) constant, K_D, is then given by Equation (2), with the fractions of the monomer and dimer obtained from Equations (3) and (4), respectively.

$$\delta_{obs} = \delta_M \times f_M + \delta_D \times f_D + \theta \times C_{tot} \quad (1)$$

$$K_D = [D]/[M]^2 \quad (2)$$

$$f_M = 1/(0.5 + 0.5\{1 + 8\,K_D C_{tot}\}^{1/2}) \quad (3)$$

$$f_D = 1 - f_M \quad (4)$$

From Figure 4 (middle plot), it is clear that the use of a linear offset term in Equation (1) ($\theta \times C_{tot}$) is mandatory for an acceptable fit of the experimental variation of the pyrrole N–H proton chemical shifts with increasing concentration of **4**. The origin of this term for the present system will be discussed below. The following parameters were obtained from the nonlinear least-squares fit of Equation (1) to the data: $\delta_M = 10.68(7)$ ppm, $\delta_D = 12.40(2)$ ppm, $K_D = 815(83)$ M^{-1}, and $\theta = 0.18(3)$ ppm M^{-1}.[37] The free-energy change for the dimerization process at 25 °C in $CDCl_3$ is thus exergonic and highly favorable: $\Delta G^{298} = -16.6(4)$ kJ mol^{-1}. Importantly, the value of K_D is three orders of magnitude higher than that measured for the mono(pyrrole) system **8**[14] under identical conditions. Our interpretation of this rather intriguing result is that a) the basic geometry of the supramolecular synthon **3** is probably near-ideal for a tight two-point hydrogen-bonding interaction, b) two molecular recognition motifs (as opposed to only one) lead to enhanced binding, and c) the conformation of **4** is in fact preorganized for self-assembly in this system. No untoward energy penalties (i.e., negative contributions to ΔS for the binding process) associated with

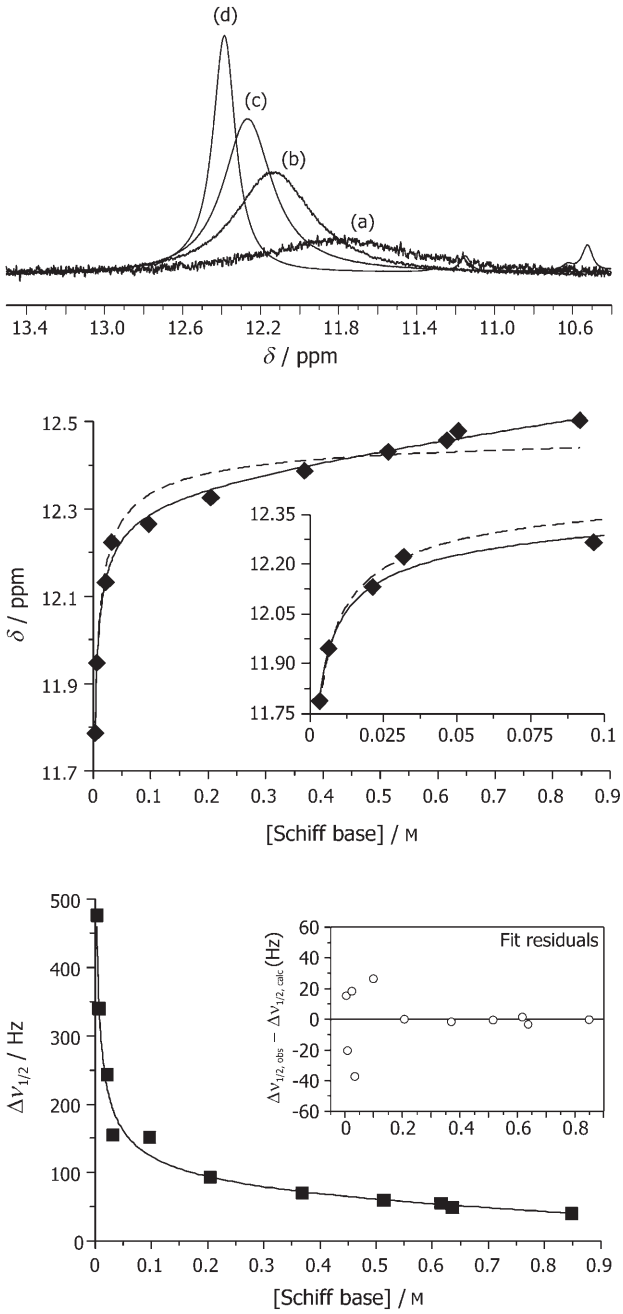

Figure 4. Top: Selected NMR spectra of **4** in the pyrrole N–H proton frequency range as a function of concentration in $CDCl_3$ at 25 °C (signal amplitudes are not plotted on the same scale): a) 3.3 mM, b) 21.3 mM, c) 96.5 mM, and d) 368 mM. Middle: fit of the chemical shift of the pyrrole N–H proton resonance as a function of concentration of **4** in $CDCl_3$ at 25 °C. The solid line is a fit to Equation (1) in the text; the dashed line is a fit to Equation (1) without the linear offset term. Bottom: Fit of the pyrrole N–H proton resonance line-width (full width at half maximum) as a function of the concentration of **4** using Equation (5).

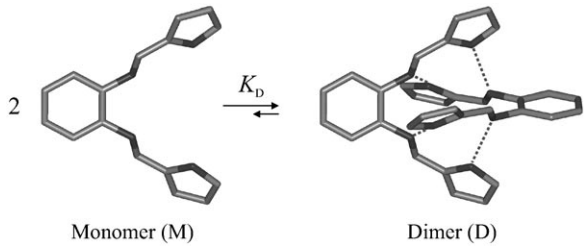

Figure 5. Diagram depicting the equilibrium self-assembly of **4**.

conformational reorganization therefore exist before two monomers of **4** may self-assemble into a dimeric structure similar (or, more likely, identical) to that of the X-ray structure (Figure 1). Our claim that **4** is preorganized for dimerization is based not only on the large value of K_D for the system, but also on the nonplanar conformation of monomeric **4** calculated in vacuo at the AM1 level of theory (vide infra). If the lowest-energy conformer of the molecule happens to be nonplanar and already of the correct shape to interact perfectly with a second monomer, then such a system is clearly preorganized for self-recognition.

Line-width analysis: The pyrrole N–H proton line-width narrows considerably (by an order of magnitude) with increasing concentration (Figure 4, lower plot). The major (nonlinear) change clearly occurs in the concentration range below 0.3 M. This marked change in line-width is due primarily to the formation of the hydrogen-bonded dimer. As noted previously for the mono(pyrrole) derivative **8**,[14] hydrogen-bond formation in the dimeric structure localizes the pyrrole N–H protons and diminishes their exchange rate until, on the NMR timescale, the slow exchange limit is reached. At concentrations higher than 0.3 M, it is evident that further more-gradual narrowing of the line-width occurs with a constant slope. This post-dimerization change in the pyrrole N–H proton line-width probably reflects the changing dielectric constant of the medium with increasing solute concentration and its indirect effect on the relaxation rate of the pyrrole N–H protons. As with Equation (1), a model was derived to fit the concentration dependence of the line-width (full width at half maximum, $\Delta\nu_{1/2}$) that specifically includes both the effect of dimerization on the line-width and the changing relaxation rate [Eq. (5)].

$$\Delta\nu_{1/2} = \Delta\nu_{1/2M} \times f_M + \Delta\nu_{1/2D} \times f_D + \psi \times C_{tot} \quad (5)$$

The fractions of the monomer and dimer in solution, f_M and f_D, are given by Equations (3) and (4), respectively. The intrinsic pyrrole N–H proton line-widths of the monomer and dimer are given by the terms $\Delta\nu_{1/2M}$ and $\Delta\nu_{1/2D}$, while the constant ψ (in units of Hz M^{-1}) quantifies the medium-induced change in the pyrrole N–H proton relaxation rate with increasing concentration. The following parameters were obtained for the fit of Equation (5) to the data: $\Delta\nu_{1/2M} = 1261(35)$ Hz, $\Delta\nu_{1/2D} = 34(6)$ Hz, $K_D = 815(56)$ M^{-1}, and $\psi = -31(13)$ Hz. Importantly, the value of K_D is equivalent to that measured from the fit of the concentration dependence of the pyrrole N–H proton chemical shift. From the fit residuals (inset to bottom graph in Figure 4), it is clear that the constant ψ allows for the line-width variation at the highest concentrations of **4** to be properly accounted for (Figure S6 gives the fit of the data by Equation (5) without the linear decay term).

Medium effects: Although the NMR spectroscopic data are indisputably well modeled by Equations (1)–(5), one concern is whether the linear offset terms are justified. If, as we suggested above, the term θ in Equation (1) takes into account monotonic changes in the dielectric constant of the medium with increasing concentration of the Schiff base, then *all* protons in the molecule must (to a first approximation) be similarly perturbed by this external change. Clearly, if the concentration dependence of the chemical shift for any magnetically unique protons in the molecule is measured, then the same value of θ should be observed in all cases. Figure 6 tests this hypothesis. The concentration dependence of the chemical shift for the imine C–H protons is shown in Figure 6a. These protons are increasingly shielded upon dimerization of **4** (as evidenced by the negative slope in the concentration range below 0.1 M) prior to experiencing monotonic deshielding in the dimer due to the change in the dielectric constant of the medium at concentrations above 0.1 M. The fit to Equation (1) is good and is described by the parameters: $\delta_M = 8.10(1)$ ppm, $\delta_D = 7.68(1)$ ppm, $K_D = 821(32)$ M^{-1}, and $\theta = 0.124(3)$ ppm M^{-1}. For the phenyl *m*-protons, the data were fit to the first-order polynomial function $\delta_{obs} = \delta_{init} + \theta \times C_{tot}$ (Figure 6b). The adjustable parameters converged to the values $\delta_{init} = 7.087(1)$ ppm and $\theta = 0.114(3)$ ppm M^{-1}. Thus, for chemically (and magnetically) unique protons in solvent-accessible environments on the outside perimeter of the dimeric structure of **4**, we find that θ is indeed constant, at about 0.11(1) ppm M^{-1}, and may correctly be attributed to concentration-dependent changes in the medium. Finally, the self-association constant K_D measured from the fit of the data for the imine C–H proton resonance (Figure 6a) is experimentally equivalent to that measured from the concentration dependence of the pyrrole N–H resonance, thus implying an internally consistent method for quantifying the self-association constant in this system.

Molecular simulations: Semi-empirical quantum mechanics simulations using methods such as AM1 are not only computationally efficient, but are widely recognized as being sufficiently accurate for simulations on medium to large hydrogen-bonded supramolecular species with both strong[11,14,38] and weak[39,40] hydrogen bonds. Using this method, our computational objectives were to: 1) fully map the region of conformational space encompassing the X-ray conformations for **4** in an effort to further understand the marked nonplanarity of each monomer conformation observed in the crystal lattice, 2) determine the structures and energies of the global and local minima accessible to **4**, 3) determine the in vacuo enthalpy of association of the dimer-

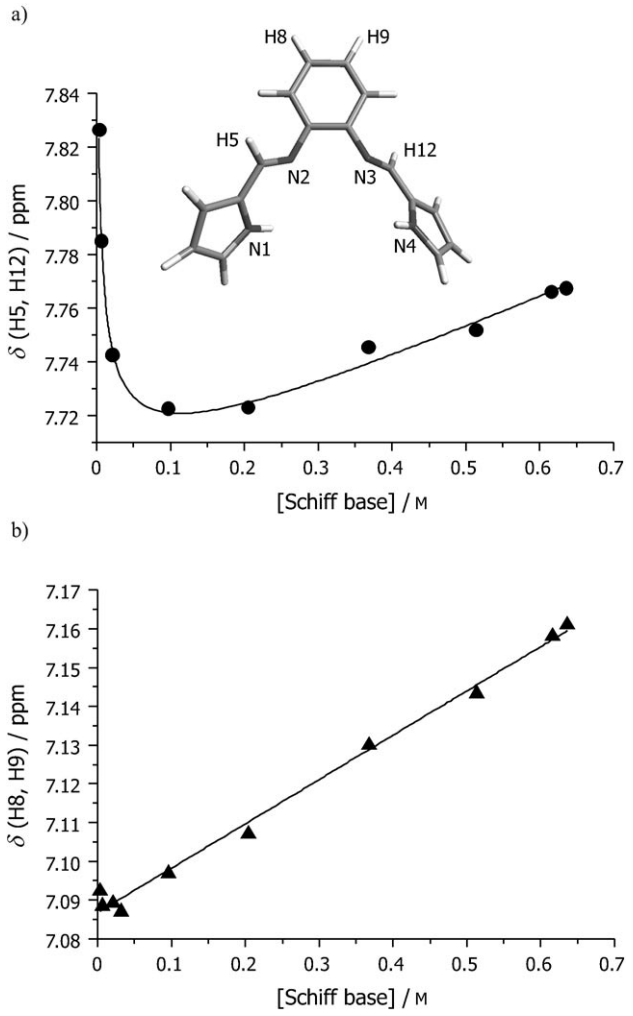

Figure 6. a) Fit of the concentration dependence of the chemical shift of the imine C–H protons at 25 °C in $CDCl_3$ to Equation (1). b) Fit of the concentration dependence of the benzene *m*-protons at 25 °C in $CDCl_3$ to a first-order polynomial function.

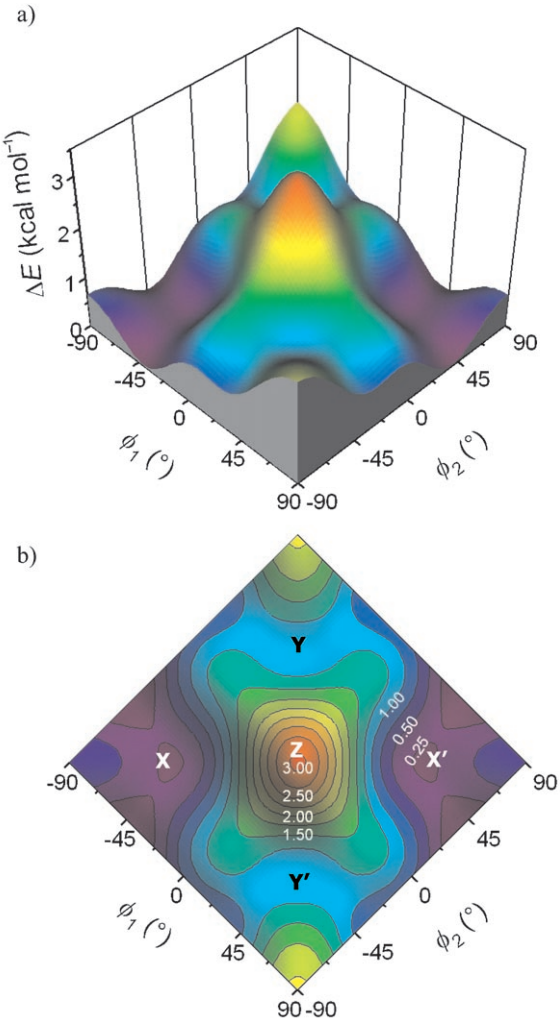

Figure 7. a) Three-dimensional plot of the variation in the relative heat of formation, ΔE, of **4** as a function of the torsion angles ϕ_1 and ϕ_2. The data were calculated at the AM1 level of theory (gas phase). b) Two-dimensional contour map of the PES showing the locations of the global energy minimum **X**, the local energy minimum **Y**, and the global energy maximum, **Z**. Inversion-related conformers have been given primed labels; torsion angles ϕ_1 and ϕ_2 are defined in Figure 8.

ic structure of **4**, and 4) delineate the electrostatics of the monomeric and dimeric forms of the compound that stabilize self-association as well as some aspects of the crystal packing between adjacent dimers in the solid state.

Low-energy conformations: Figure 7a shows a three-dimensional plot of the potential energy surface (PES) that spans the conformational space incorporating the most relevant conformers of **4** (the torsion angles ϕ_1 and ϕ_2 are defined graphically in Figure 8). From the contour map of the surface (Figure 7b), a center of inversion exists at the coordinate ϕ_1, $\phi_2 = 0°$. This corresponds to the global maximum (**4Z**, Figure 8) with a heat of formation some 2.86(2) kcal mol^{-1} higher than that of the lowest energy conformer (**4X**) found at ϕ_1, $\phi_2 = -49.8°$. Importantly, conformer **4X** has a highly nonplanar, twisted architecture that is remarkably similar in geometry to the independent monomers found in the X-ray structure of **4** (Figure 9a). This strongly suggests that dimerization of **4** does not require a pronounced conformational adjustment and that the lowest-energy conformation has the correct geometry for self-assembly by hydrogen-bond formation into the experimentally observed dimeric structure. Together with the X-ray data, our AM1 simulations therefore indicate that **4X** is conformationally preorganized for this particular molecular recognition event.

Several other interesting conformations are energetically feasible for **4**. Thus, a local minimum with a nonplanar domed conformation (both pyrrole N–H groups pointing above or below the molecular mean plane) was located by the grid search of conformational space (**4Y**). This conformation is 0.83 kcal mol^{-1} higher in energy than the global minimum. The transition state ($\Delta E = 1.5$ kcal mol^{-1}) connecting minima **4X** and **4Y** corresponds to a structure in which one pyrrole ring is canted out of the mean molecular plane ($\phi_1 = -49°$) while the other remains coplanar with re-

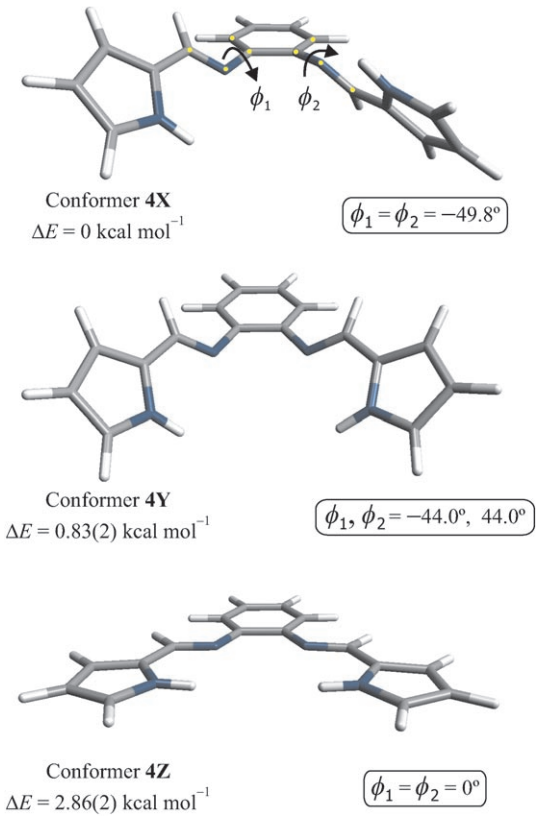

Figure 8. Structures and relative heats of formation of the C_2-symmetric conformations **4X** and **4Z** and the C_1-symmetric conformer **4Y** taken from the AM1-calculated potential energy surface for monomeric **4** shown in Figure 8. The torsion angles ϕ_1 and ϕ_2 are defined using **4X** for illustration.

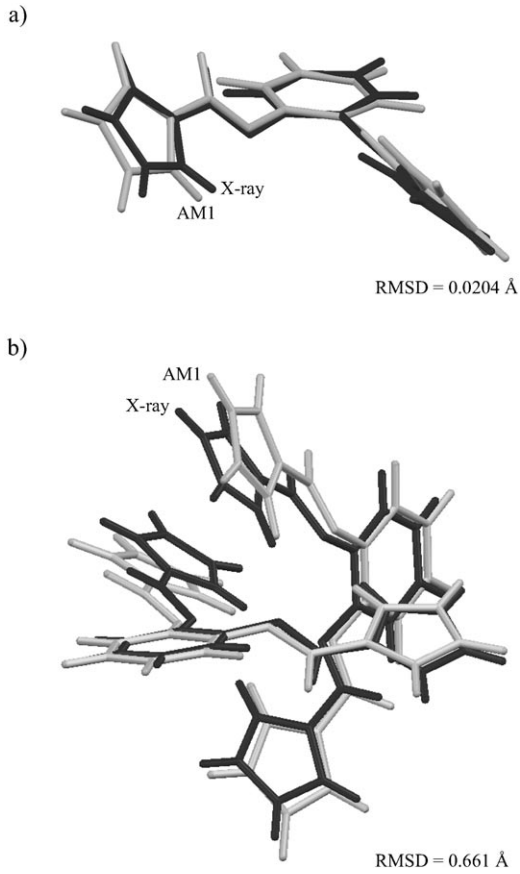

Figure 9. a) Root-mean-square fit of the X-ray structure of **4** (molecule B) to the AM1-calculated conformation **4X** (in vacuo) of the monomeric Schiff base derivative. b) Root-mean-square fit of the X-ray structure of **4** (molecules A and B) to the AM1-calculated structure of the dimer in the gas phase. All atoms were included in the least-squares fitting procedure in both cases.

spect to the benzene ring ($\phi_2 = 0°$). The low barrier for the transition state (saddle-point) reflects the fact that the most strained conformation of the compound has the two pyrrole N–H groups pointing directly at one another (**4Z**). As soon as one pyrrole ring flips out of the mean molecular plane, steric strain is partly relieved. Full relief of the steric strain engendered by nonbonded repulsion between the pyrrole N–H groups occurs if both pyrrole rings are canted out of plane and in opposite directions (conformer **4Z** → **4X**). Interestingly, our AM1 simulations suggest that the bond order for the central C–N bond of the torsion angles ϕ_1 and ϕ_2 is much closer to one than two. Specifically, the Wiberg bond order[41] calculated for **4X** (1.04) is only marginally less than that calculated for **4Z** (1.06), thus suggesting that the barrier to rotation about ϕ_1 and ϕ_2 should be close to that for a normal C–N single bond. A further indication of the low C–N bond order is the fact that the energy of the conformation calculated with $\phi_1 = \phi_2 = 90°$ is only around 0.6 kcal mol^{-1} (Figure 7). For a strongly delocalized structure with a bond order closer to two, such a conformation would be expected to have one of the highest energies for the system, not one of the lowest.

Theoretical versus experimental structures: As shown in Figure 9, the AM1-calculated structures of monomeric and dimeric **4** are fundamentally good when compared with the relevant X-ray structures using least-squares fitting techniques. If we take into account the fact that the simulations include only the valence electrons and operate in vacuo (local distortions of the experimental conformers caused by crystal packing interactions, such as those illustrated in Figure 4, are thus excluded), then the fact that the differences between the experimental and theoretical structures amount to less than 1 Å for all atoms in each case is remarkable. Furthermore, if we consider some key intermolecular interactions, we find that the mean N–H···N and $N_{donor}\cdots N_{acceptor}$ hydrogen-bond distances in the calculated structure of the dimer (Figure 9b) are 2.56 and 3.47 Å, respectively, and thus compare reasonably well with the analogous values determined crystallographically (2.04(3) and 2.93(3) Å). Together with the acceptable conformation calculated for the dimeric structure of **4**, we conclude that AM1 provides a practical and computationally efficient method for analyzing the conformational structures, most probably the relative energies, and possibly some of the fundamentals of the H-bonding in-

teractions in this rather complex experimental system. It is worth noting that the calculation of the PES for **4** (with 19^2 conformers, Figure 7) would be prohibitively costly in both computational time and machine infrastructure, with no guarantee of improved structural accuracy,[42] for any HF or DFT methods with basis sets $\geq$ 3-21G[43] in size.

Electrostatics: Previous work by our group[11,14] has shown that complementary electrostatic interactions are probably the key driving force for the self-assembly of pyrrole-imine systems **3** both in the solid state and in solution. The Mulliken populations[44] (partial charges) computed at the AM1 level of theory for the monomeric and dimeric forms of **4** confirm this notion (Figure 10). Specifically, the pyrrole N–

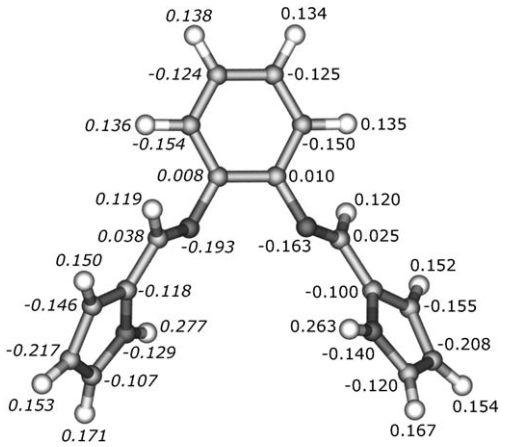

Figure 10. Symmetry-unique Mulliken partial-charge distributions (in electron units) calculated at the AM1 level of theory for the D_2-symmetric dimeric structure of **4** (italics font, left half of molecule) and the C_2-symmetric monomer (right half of molecule).

H hydrogen partial charge (+0.263) complements the partial charge of the imine C=N nitrogen (−0.163) in the monomer. Dimer formation clearly also favors polarization of these key functional groups, particularly the imine C=N unit, where the charge separation increases from $C^{0.025}$=$N^{-0.163}$ in the monomer to $C^{0.038}$=$N^{-0.193}$ in the hydrogen-bonded dimer. As might be expected, the calculated Wiberg bond orders[41] for the C=N and pyrrole N–H bonds confirm the above polarization effects resulting from hydrogen-bond formation. Thus, the C=N bond order decreases from 1.84 in the monomer to 1.82 in the dimer, while the N–H bond order decreases from 0.882 in the monomer to 0.873 in the dimer. These changes are mirrored by red shifts in the calculated vibrational frequencies of these bonds. Specifically, dimerization favors a decrease in the intense antisymmetric pyrrole N–H stretching vibration from 3512 cm^{-1} in the monomer to 3479 cm^{-1} in the dimer. The antisymmetric C=N stretching mode is similarly shifted from 1921 cm^{-1} in the monomer to 1909 cm^{-1} in the dimer. While the calculated vibrational frequencies are not particularly accurate and differ by as much as 300 cm^{-1} from the experimental values (Supporting Information), this limitation of the AM1 method is well known and is paralleled by similar, though smaller, over-estimations of calculated vibrational frequencies by more rigorous ab initio methods.[45] Notwithstanding this, the simulations still afford a qualitatively correct measure of the electronic structure perturbations brought about by dimerization in this system.

Self-assembly thermodynamics: The dimerization of **4** measured by NMR spectroscopy in $CDCl_3$ solution is clearly exergonic ($\Delta G < 0$, vide supra). For credibility, any theoretical simulation of this system would need to give a comparable result. To compute the Gibbs energy change and enthalpy change for self-assembly of **4**, we first calculated the structure of the dimer using the X-ray coordinates as input. We then moved the constituent monomers apart to a distance greater than 11 Å and recalculated the geometries of the noninteracting molecules. A full frequency analysis of each system was employed to evaluate the thermochemical parameters at 298 K. The enthalpy of association, ΔH_{assoc}, was calculated from Equation (6), where ΔH_f(dimer) is the heat of formation at 298 K of the dimer and $\Delta H_f^{\#}$ is the heat of formation of the noninteracting system.

$$\Delta H_{assoc} = \Delta H_f(\text{dimer}) - \Delta H_f{}^{\#} \quad (6)$$

A similar equation was used to evaluate the Gibbs function for self-assembly in the gas phase. In effect, Equation (6) is equivalent to applying a counterpoise correction[46] for the basis set superposition error that typically affects the calculated binding energies of dimers in all-electron basis set simulation methods. From the thermodynamic data listed in Table 3, we calculate $\Delta H_{assoc} = -29.2\ kJ\,mol^{-1}$, $\Delta G_{assoc} = -21.9\ kJ\,mol^{-1}$, and $\Delta S_{assoc} = -24.3\ J\,K^{-1}\,mol^{-1}$ at 298 K. The negative entropy term is not only of a sensible magnitude but indeed perfectly correct for a system in which two reactant species associate to form a single product. Remarkably, the gas-phase free-energy change calculated for self-assembly of **4** is in very good agreement with the value measured by NMR spectroscopy ($\Delta G_{assoc} = -16.6(4)\ kJ\,mol^{-1}$). This confirms the suitability of AM1 for such calculations, in agreement with our previous findings,[38] and probably reflects the fact that the dielectric constant of $CDCl_3$ (4.81 D) is not overly different from the gas-phase di-

Table 3. AM1-calculated conformational and frontier MO energies (at 298 K) for various structural forms of **4**.

Conformation	ΔH_f[a]	ΔG_f[a]	E_{HOMO}[b]	E_{LUMO}[b]	ΔE_{HL}[b,c]
twisted, **4X**	154.04	298.33	−8.327	−0.3810	7.946
domed, **4Y**	154.87	299.21	−8.272	−0.4626	7.810
flat, **4Z**	156.91	304.00	−8.136	−0.7619	7.374
D_2 dimer	302.71	605.96	−8.245	−0.5987	7.647
4X, **4X**[d]	309.68	611.20	−8.272	−0.5170	7.755

[a] Energy in kcal mol^{-1}. [b] Energy in eV. [c] $E_{LUMO} - E_{HOMO}$. [d] Two twisted monomers separated by 11 Å.

electric constant (1.0 D). Importantly, our finding that the experimental value of ΔG_{assoc} is only slightly less than that calculated for **4** in the absence of solvent suggests that solvation of the *dimer* by a non hydrogen-bonding solvent might marginally weaken the molecular recognition interactions that stabilize the supramolecular structure. Since $CDCl_3$ has a dipole moment, this subtle effect may derive from perturbation of the complementary electrostatics that seemingly govern hydrogen bonding in this system. Alternatively, an entropy penalty related to desolvation of the monomers upon dimerization in the experimental system, which is obviously unaccounted for in the gas phase simulation, might be at work.

Molecular orbitals: The MO energies listed in Table 3 for different monomer conformations of **4** as well as the hydrogen-bonded dimer suggest that the electronic structure of the system is fairly sensitive to both structural distortion and to dimer formation. The twisted, highly nonplanar lowest energy conformer of the Schiff base **4X** has the largest HOMO–LUMO energy gap. The frontier MO splitting, ΔE_{HL}, for **4X** is seen to be larger than that for **4Z** (planar conformation) by more than 0.5 eV. For the series of conformers **4X**, **4Y**, and **4Z**, the HOMO energy systematically increases while the LUMO energy systematically decreases. Clearly, the conformation-dependence of ΔE_{HL} reflects modulation of the π-electron delocalization with the degree of distortion of the structure. A convenient way to further analyze this trend is to evaluate how bond orders for key bonds in the structure change when the conformation distorts from planarity. Thus, we found that the calculated C=N bond orders were 1.841, 1.833, and 1.814 for conformers **4X**, **4Y**, and **4Z**. The slight decrease in C=N bond order with increasing planarity of the conformation is consistent with increased π-electron delocalization. However, it is noteworthy that even the nonplanar conformer **4X** exhibits extensive π-electron delocalization, as evidenced by the HOMO, which spans the entire structure (Figure 11 a).

Finally, an important question is how tightly mingled are the electronic structures of the monomers that make up the dimer in this hydrogen-bonded system? Previous calculations on more weakly hydrogen-bonded dimers suggest that considerable mixing occurs.[14] In the present system, Figure 11 b clearly shows that the dimer of **4** has an electronic structure that is not merely the sum of the two independent monomers. If this were the case, the HOMO would reside entirely on one monomer component of the dimer and the HOMO−1 (not shown) on the other. The fact that the HOMO is fully delocalized over both monomers within the dimer (other filled π MOs behave similarly) indicates that the interlocked Schiff base units become electronically mixed upon dimer formation. Considering the fact that the mean plane of one monomer unit is almost orthogonal to that of the other (86.0°) and, furthermore, that the monomers are linked by noncovalent bonds, this level of π-orbital mixing (and thus π-electron delocalization) is quite remarkable.

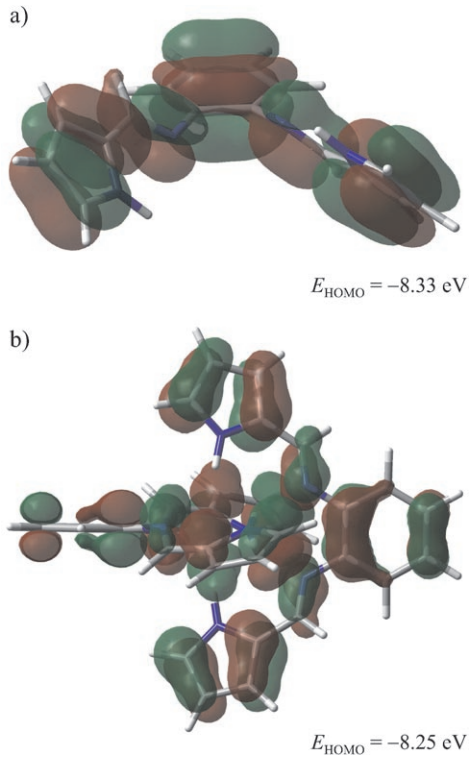

Figure 11. a) HOMO for the AM1-calculated C_2-symmetric monomeric structure **4X**. b) HOMO for the D_2-symmetric dimer.

Conclusion

We have obtained novel X-ray structural data for a bis(pyrrole) Schiff base derivative synthesized by the condensation of 1,2-diaminobenzene and pyrrole-2-carboxaldehyde (compound **4**). The crystal structure shows that dimers are formed through complementary sets of hydrogen bonds between the pyrrole N−H donor groups and imine N=C acceptor groups of the interacting monomers. The crystal lattice exhibits an unusual packing pattern for the dimers, which assemble into layers of columns whose axes are collinear with the crystallographic *a* axis. We have established that this intriguing packing leaves small H_2-sized voids (with two geometries) between the layers of dimers. However, the absence of bona fide channels within the lattice probably prevents hydrogen gas uptake (sorption) by the microcrystalline solid, despite the use of hydrogen pressures up to 10 bar.

From the concentration dependence of key resonances in the ^{1}H NMR spectrum of **4**, we have used nonlinear curve-fitting methods to delineate the self-assembly process for **4** in fluid solution and have established that dimer formation is highly exergonic ($\Delta G_{assoc} = -16.6$ kJ mol^{-1}). Semiempirical MO calculations at the AM1 level of theory indicate that complementary hydrogen bonding (molecular recognition) in this system is driven by favorable electrostatic interactions. Thermochemical analysis of the self-assembly process for **4** in vacuo using AM1 affords a remarkably good prediction of ΔG_{assoc} for the reaction (−21.9 kJ mol^{-1}). Part of the

success of the in vacuo AM1 simulation may be due to the fortuitously small contribution that solvation makes to the thermodynamics of the process in the experimental system. Finally, our AM1 simulations of the potential energy surface for monomeric **4** indicate that the lowest energy conformer has a twisted nonplanar structure that is clearly preorganized for self-assembly into a dimeric supramolecular structure.

Experimental Section

General details and synthesis: Hexane and dichloromethane (BDH) were distilled from sodium metal and calcium hydride, respectively, before use. Ethanol (96%, BDH), pyrrole-2-carboxaldehyde, and 1,2-phenylenediamine (both from Aldrich) were used as received. Electronic spectra were recorded with a Perkin–Elmer Lambda 45 double beam spectrophotometer using CH_2Cl_2 solutions in 1.0 cm path length cuvettes. Samples for IR spectroscopy were KBr mulls of polycrystalline material. FT-IR spectra were recorded with a Perkin–Elmer Spectrum One spectrometer (four scans; spectral resolution: 1.0 cm^{-1}). Compound **4** was synthesized from 1,2-phenylenediamine (1.600 g, 15.0 mmol) and pyrrole-2-carboxaldehyde (2.853 g, 30.0 mmol) in refluxing ethanol (15 mL) following the literature method of Jones.[47] Single crystals of **4** suitable for X-ray diffraction studies were grown by slow diffusion of hexane into a dichloromethane solution of **4**, or by slow evaporation of the solvent (ethanol). ^{1}H NMR spectroscopic data for **4** were consistent with those reported in the literature (Supporting Information).[6]

X-ray crystallography: X-ray diffraction data for a pale-yellow rectangular block with the approximate dimensions $0.4\times0.6\times0.7$ mm^3 were collected with an Oxford Diffraction Xcalibur2 CCD four-circle diffractometer equipped with an Oxford Instruments Cryojet operating at 100(2) K. The data were collected at a crystal-to-detector distance of 60 mm using omega scans at $\theta=29.327°$ with 30 s exposures taken at 2.20 kW X-ray power with 0.60° frame widths. The data were reduced with the program CrysAlis RED[48] using outlier rejection, scan speed scaling, as well as standard Lorentz and polarization correction factors. A total of 65453 reflections were merged to give 40466 unique data with an average redundancy of 1.6 and a mean $F^2/\sigma F^2$ of 14.61. The internal R index for the data set after reduction was 0.03(3) and the resolution of the data was to 0.72 Å. The structure was solved in the monoclinic space group $C2/c$ using direct methods in WinGX's[49] implementation of SHELXS-97.[50] All non-H atoms were located in the electron density map and were refined anisotropically with SHELXL-97.[50] The data set was of sufficiently high quality that all H atoms were located in the final difference Fourier synthesis cycle. The coordinates of the hydrogen atoms attached to the pyrrole nitrogen atoms of **4** were refined isotropically without constraints; however, the isotropic U_{ij} values were fixed at 1.2-times the U_{eq} values of the nitrogen atoms. All other H atoms were calculated using the standard riding model of SHELXL-97 (HFIX 43 instruction). Table S1 lists the full crystal and data collection parameters for **4.**

CCDC-601917 contains the supplementary crystallographic data for this paper. These data can be obtained free of charge from the Cambridge Crystallographic Data Centre via www.ccdc.cam.ac.uk/data_request/cif.

Crystal data: $C_{16}H_{14}N_4$, $M=262.31$ $g\,mol^{-1}$, $T=100(2)$ K, $\lambda=0.71073$ Å, monoclinic, $C2/c$, $a=34.778(10)$, $b=17.018(11)$, $c=14.094(4)$ Å, $\beta=94.40(2)°$, $V=8317(6)$ $Å^3$, $Z=24$, $\rho_{calcd}=1.257$ $g\,cm^{-3}$, $\mu=0.08$ mm^{-1}, reflections collected = 31465, unique reflections = 10365, observed reflections = 8630 ($R_{int}=0.022$), goodness-of-fit on $F^2=1.06$, $R_1=0.044$ ($F^2>2\sigma(F^2)$), $wR_2=0.113$ (F^2), largest difference peak and hole = 0.28 and -0.21 e $Å^{-3}$.

Dimerization of 4 studied by NMR spectroscopy: NMR spectra for **4** were recorded as a function of concentration in $CDCl_3$ at 25 °C with a Varian Unity Inova 500 MHz spectrometer operating at a transmitter frequency of 499.983 MHz. Solutions were prepared by dissolving from 0.5 mg up to 130 mg of polycrystalline material in 600 μL of $CDCl_3$ dried over activated neutral alumina. Standard pulse sequences were used (128 scans, spectral width = 12604.38 Hz, spectral resolution = 0.264265 Hz). An exponential line-broadening factor of 1.061 was used during Fourier transformation of the data with the program SpinWorks 2.5.1.[51] The pyrrole N–H signal (at about $\delta=12$ ppm) was fit to a Voigt line-shape function[52] in each case and the resonant frequency, intensity, and line width determined accurately by nonlinear least-squares regression using the program PEAKFIT v4.0 (Table S2).[53]

Molecular simulations: AM1[54] geometry optimization calculations were carried out with ArgusLab 4.0.1[55] and Gaussian 03W[56] using the X-ray coordinates of **4** as input. Spin-restricted wave functions were used on the lowest-lying doublet states of the X-ray structures (monomer and H-bonded dimer), which were analyzed by single-point calculations as well as full geometry optimizations with the default convergence criteria. Frequency calculations (298.15 K) were performed on each optimized structure. No imaginary vibrational modes were found for the nonplanar C_2-symmetric conformation of **4**, thus confirming the fact that this conformer is a true minimum on the potential energy surface. In contrast, the planar C_2-symmetric conformation yielded one imaginary frequency.

A relaxed scan of the potential energy surface (PES) was performed at the AM1 level of theory for monomeric **4** by counter-rotating the pyrrole-imine units from −90 to 90° in 10° increments, producing a total of 19^2 starting conformations for refinement. The torsion angles ϕ_1 and ϕ_2 were defined as the adjacent pair of C=C−C=N angles with the C=C bond *not* common to both (e.g., C6b−C7b and C11b−C10b in molecules A and B of the X-ray structure). A maximum of 2000 least-squares cycles with a root-mean-square gradient termination cutoff of 0.01 $kcal\,Å^{-1}\,mol^{-1}$ was used for geometry optimization with the Polak–Ribiere conjugate gradient algorithm in HyperChem 6.03.[57] The three-dimensional grid of enthalpy of formation data was analyzed in relative energy format, ΔE, using the global energy minimum as the zero reference. The program KyPlot 3.0[58] was used with a thin plate smoothing spline regression to fit the 3D data (a second-order penalty derivative and equivalent bandwidth, i.e., smoothing parameter, of 0.1 were employed with a calculation step set at 90 x and y grid divisions).

Acknowledgments

We gratefully acknowledge financial support from the University of KwaZulu-Natal, SASOL, and the National Research Foundation (NRF, Pretoria). Any opinion, findings and conclusions or recommendations expressed in this paper are those of the authors and therefore the NRF does not accept any liability in regard thereto. The authors also wish to thank Prof. Len Barbour and Gareth Lloyd of the University of Stellenbosch for assaying the H_2 sorption behavior of **4**.

[1] J. H. Weber, *Inorg. Chem.* **1967**, *6*, 258–262.
[2] C. Stern, F. Franceschi, E. Solari, C. Floriani, N. Re, R. Scopelliti, *J. Organomet. Chem.* **2000**, *593*, 86–95.
[3] A. Bacchi, M. Carcelli, L. Gabba, S. Ianelli, P. Pelagatti, G. Pelizzi, D. Rogolino, *Inorg. Chim. Acta* **2003**, *342*, 229–235.
[4] a) N. A. Bailey, S. E. Hull, *Cryst. Struct. Commun.* **1976**, *5*, 447–450; b) C. Kabuto, T. Kikuchi, H. Yokoi, M. Iwaizumi, *Chem. Lett.* **1984**, 573–574; c) J. Sakon, A. Reiter, K. Bowman-Mertes, F. Takusagawa, *Acta Crystallogr. Sect. C* **1989**, *45*, 1311–1314.
[5] L. Yang, Q. Chen, Y. Li, S. Xiong, G. Li, J. S. Ma, *Eur. J. Inorg. Chem.* **2004**, 1478–1487.
[6] F. Franceschi, G. Guillemot, E. Solari, C. Floriani, N. Re, H. Birkedal, P. Pattison, *Chem. Eur. J.* **2001**, *7*, 1468–1478.
[7] S. D. Reid, A. J. Blake, W. Kockenberger, C. Wilson, J. B. Love, *Dalton Trans.* **2003**, 4387–4388.
[8] C. D. Berube, S. Gambarotta, G. P. A. Yap, P. G. Cozzi *Organometallics* **2003**, *22*, 434–439.

[9] U. Mueller-Westerhoff, A. L. Rheingold, M. B. Allen, *Private Communication to the CSD*, 1996, Ref. code NACRAK; F. H. Allen, *Acta Crystallogr. Sect. B* **2002**, *58*, 380–388.
[10] Z. Wu, Q. Chen, S. Xiong, B. Xin, Z. Zhao, L. Jiang, J. S. Ma, *Angew. Chem.* **2003**, *115*, 3393–3396; *Angew. Chem. Int. Ed.* **2003**, *42*, 3271–3274;.
[11] O. Q. Munro, G. L. Camp, *Acta Crystallogr. Sect. C* **2003**, *59*, o672–o675.
[12] J. L. Sessler, G. Berthon-Gelloz, P. A. Gale, S. Camiolo, E. V. Anslyn, P. Anzenbacher Jr., H. Furuta, G. J. Kirkovits, V. M. Lynch, H. Maeda, P. Morosini, M. Scherer, J. Shriver, R. S. Zimmerman, *Polyhedron* **2003**, *22*, 2963–2983.
[13] In compound **7**, adventitious water is included in the H-bonding network to give a polymeric structure.
[14] O. Q. Munro, S. D. Strydom, C. Grimmer, *New J. Chem.* **2004**, *28*, 34–42.
[15] G. R. Desiraju, T. Steiner, *The Weak Hydrogen Bond in Structural Chemistry and Biology*, Oxford University Press, **1999**.
[16] T. Steiner, *Chem. Commun.* **1997**, 727–734.
[17] F. H. Allen, W. D. S. Motherwell, P. R. Raithby, G. P. Shields, R. Taylor, *New J. Chem.* **1999**, *23*, 25–34.
[18] Shorter H···acceptor distances do not necessarily correlate with stronger hydrogen bonds because of crystal packing effects, orientation angles, and other intermolecular interactions.
[19] Strictly speaking, the mean hydrogen-bond distance of **4** is equal (within an error bound of 4σ) to the average distance of 2.16(6) Å for the seven compounds listed in Table 2.
[20] T. Steiner, *Angew. Chem.* **2002**, *114*, 50–80; *Angew. Chem. Int. Ed.* **2002**, *41*, 48–76.
[21] S. Matsui, Y. Yoshida, Y. Takagi, T. P. Spaniol, J. Okuda, *J. Organomet. Chem.* **2004**, *689*, 1155–1164.
[22] N. Davidović, D. Matković-Čalogović, Z. Popović, L. Fišer-Jakić, *Acta Crystallogr. Sect. C* **1999**, *55*, 119–120.
[23] R. M. Bellabarba, P. T. Gomes, S. I. Pascu, *Dalton Trans.* **2003**, 4431–4436.
[24] T. D. Hamilton, L. R. MacGillivray, *Adv. Phys. Org. Chem.* **2005**, *40*, 109–152.
[25] a) J. L. Rowsell, O. M. Yaghi, *Angew. Chem.* **2005**, *117*, 4748–4758; *Angew. Chem. Int. Ed.* **2005**, *44*, 4670–4679; b) S. Kitagawa, K. Uemura, *Chem. Soc. Rev.* **2005**, *34*, 109–119; c) B. Kesanli, W. Lin, *Coord. Chem. Rev.* **2003**, *246*, 305–326.
[26] L. Dobrzanska, G. O. Lloyd, H. G. Raubenheimer, L. J. Barbour, *J. Am. Chem. Soc.* **2006**, *128*, 698–699.
[27] H. Chun, D. N. Dybtsev, H. Kim, K. Kim, *Chem. Eur. J.* **2005**, *11*, 3521–3529.
[28] a) Y. Li, R. T. Yang, *J. Am. Chem. Soc.* **2006**, *128*, 726–727; b) T. Sagara, J. Ortony, E. Ganz, *J. Chem. Phys.* **2005**, *123*, 214707.
[29] M. L. Connolly, *J. Am. Chem. Soc.* **1985**, *107*, 1118–1124.
[30] L. J. Barbour, *J. Supramol. Chem.* **2001**, *1*, 189–191.
[31] OSCAIL Version X, P. McArdle, *J. Appl. Crystallogr.* **1995**, *28*, 65.
[32] P. McArdle, D. Cunningham, *J. Appl. Crystallogr.* **2000**, *33*, 993.
[33] J. L. Atwood, L. Barbour, P. K. Thallapally, T. B. Wirsig, *Chem. Commun.* **2005**, 51–53.
[34] The same polymorph of **4** was obtained by slow evaporation of a solution of the Schiff base in ethanol or diffusion of hexane into a dichloromethane solution of the compound, which suggests that the *C*2/*c* polymorph is thermodynamically preferred. Phase changes and polymorphism may well not be energetically feasible in this system.
[35] T. Friščić, L. R. MacGillivray, *Chem. Commun.* **2005**, 5748–5750.
[36] R. K. Harris, *Nuclear Magnetic Resonance Spectroscopy: A Physicochemical View*, 2nd ed., Longman Scientific & Technical, Harlow, **1986**.
[37] The sum of squares of errors (sse) and estimated standard deviation (esd) were more than acceptable ($sse = 3.06 \times 10^{-3}$ and $esd = 1.96 \times 10^{-2}$).
[38] O. Q. Munro, K. du Toit, S. E. Drewes, N. R. Crouch, D. A. Mulholland, *New J. Chem.* **2006**, *30*, 197–207.
[39] O. Q. Munro, L. Mariah, *Acta Crystallogr. Sect. B* **2004**, *60*, 598–608.
[40] a) Z. Hajnal, G. M. Keserü, K. Simon, *J. Mol. Struct.: THEOCHEM* **1999**, *463*, 169–174; b) R. Thaimattam, F. Xue, J. A. R. P. Sarma, T. C. W. Mak, G. R. Desiraju, *J. Am. Chem. Soc.* **2001**, *123*, 4432–4445.
[41] M. W. Wong, M. J. Frisch, K. B. Wiberg, *J. Am. Chem. Soc.* **1991**, *113*, 4776–4782.
[42] To check the accuracy of the AM1 simulations, we ran a simulation of the D_2-symmetric dimer structure of **4** at the B3LYP/6-31+G* level of theory and found that the mean H···A distance is shorter (1.998(0) Å) than that of the X-ray structure (2.04(3) Å).
[43] J. S. Binkley, J. A. Pople, W. J. Hehre, *J. Am. Chem. Soc.* **1980**, *102*, 939–947.
[44] R. S. Mulliken, *J. Chem. Phys.* **1955**, *23*, 1833–1840.
[45] J. B. Foresman, A. Frisch, *Exploring Chemistry with Electronic Structure Methods*, 2nd ed., Gaussian, Inc., Pittsburgh, PA, **1996**.
[46] S. Simon, M. Duran, J. J. Dannenberg, *J. Chem. Phys.* **1996**, *105*, 11024–11031.
[47] C. J. Jones in *Inorganic Experiments* (Ed.: J. D. Woollins), VCH, Cambridge, **1994**, pp. 127–132.
[48] CrysAlis CCD and CrysAlis RED, Version 170, Oxford Diffraction Ltd., 20 Nuffield Way, Abingdon, OX14 1RL, UK, **2002**.
[49] L. J. Farrugia, *J. Appl. Crystallogr.* **1999**, *32*, 837–837.
[50] G. M. Sheldrick, SHELXS-97 and SHELXL-97, Programs for the Solution and Refinement of Crystal Structures, University of Göttingen, Germany, **1997**.
[51] K. Marat, SpinWorks 2.5.1, Program for Processing NMR Data, University of Manitoba, Canada, **2005**.
[52] O. Q. Munro, S. C. Shabalala, N. J. Brown, *Inorg. Chem.* **2001**, *40*, 3303–3317.
[53] PeakFit Version 4.0, AISN Software Inc., SPSS Science, Chicago, IL 60606-6307, USA.
[54] M. J. S. Dewar, E. G. Zoebisch, E. F. Healy, J. J. P. Stewart, *J. Am. Chem. Soc.* **1985**, *107*, 3902–3909.
[55] M. A. Thompson, Planaria Software LLC, Seattle, WA, http://www.arguslab.com, **2005**.
[56] Gaussian 03 (Revision C.02), M. J. Frisch, G. W. Trucks, H. B. Schlegel, G. E. Scuseria, M. A. Robb, J. R. Cheeseman, V. G. Zakrzewski, J. A. Montgomery, R. E. Stratmann, J. C. Burant, S. Dapprich, J. M. Millam, A. D. Daniels, K. N. Kudin, M. C. Strain, O. Farkas, J. Tomasi, V. Barone, M. Cossi, R. Cammi, B. Mennucci, C. Pomelli, C. Adamo, S. Clifford, J. Ochterski, G. A. Petersson, P. Y. Ayala, Q. Cui, K. Morokuma, D. K. Malick, A. D. Rabuck, K. Raghavachari, J. B. Foresman, J. Cioslowski, J. V. Ortiz, B. B. Stefanov, G. Liu, A. Liashenko, P. Piskorz, I. Komaromi, R. Gomperts, R. L. Martin, D. J. Fox, T. Keith, M. A. Al-Laham, C. Y. Peng, A. Nanayakkara, C. Gonzalez, M. Challacombe, P. M. W. Gill, B. G. Johnson, W. Chen, M. W. Wong, J. L. Andres, M. Head-Gordon, E. S. Replogle, and J. A. Pople, Gaussian, Inc., Pittsburgh PA, **2003**.
[57] HyperChem, Version 6.03. Hypercube Inc., 1115 NW 4th Street, Gainsville, FL 32601-4256, USA, **2000**.
[58] KyPlot Version 3.0, Kyence Inc., http://kyence.com/, **2002**.

Received: March 22, 2006
Revised: June 12, 2006
Published online: September 8, 2006

